Recent progress on photon-counting superconducting detectors for submillimeter astronomy

J. D. Teufel[a], T. R. Stevenson[b], W.-T. Hsieh[b,d], M. J. Li[b], K.W. Rhee[e], C. M. Stahle[b], E. J. Wollack[c], A. Aassime[f] , P. Delsing[f], P. Wahlgren[f], D. E. Prober[a], and R. J. Schoelkopf*[a]

[a]Dept. of Applied Physics and Physics, Yale University, P.O. Box 208284, New Haven, CT 06520
[b]NASA/GSFC, Detector Systems Branch, Code 553, Greenbelt, MD 20771
[c]NASA/GSFC, Infrared Astrophysics Branch, Code 685, Greenbelt, MD 20771
[d] Raytheon ITSS, Lanham, MD 20703
[e]Naval Research Laboratory, Electronics Sciences & Technology, Washington DC 20375
[f]Dept. of Microelectronics and Nanoscience, MC2, Chalmers University of Technology and Göteborg University, S-41296 Gothenburg, Sweden

ABSTRACT

We are developing superconducting direct detectors for submillimeter astronomy that can in principle detect individual photons. These devices, Single Quasiparticle Photon Counter (SQPC), operate by measuring the quasiparticles generated when single Cooper-pairs are broken by absorption of a submillimeter photon. This photoconductive type of device could yield high quantum efficiency, large responsivity, microsecond response times, and sensitivities in the range of 10^{-20} Watts per root Hertz. The use of antenna coupling to a small absorber also suggests the potential for novel instrument designs and scalability to imaging or spectroscopic arrays. We will describe the device concept, recent results on fabrication and electrical characterization of these detectors, issues related to saturation and optimization of the device parameters. Finally, we have developed practical readout amplifiers for these high-impedance cryogenic detectors based on the Radio-Frequency Single-Electron Transistor (RF-SET). We will describe results of a demonstration of a transimpedance amplifier based on closed-loop operation of an RF-SET, and a demonstration of a wavelength-division multiplexing scheme for the RF-SET. These developments will be a key ingredient in scaling to large arrays of high-sensitivity detectors.

Keywords: submillimeter, superconducting detector

1. INTRODUCTION

To take advantage of very low background photon rates, space-based far infrared or submillimeter-wave interferometers will require large advances in detector sensitivity and speed. Integration of photon-counting detectors with low power readout electronics to make large-format arrays is desired. The Single Quasiparticle Photon Counter (SQPC) is a type of superconducting direct detector, which has been proposed[1] to meet these requirements. This paper gives an overview of operation principles of the SQPC, the current state of development of this device, and its potential advantages.

2. DETECTOR CONCEPT AND FABRICATION

The SQPC is an antenna-coupled Superconducting Tunnel Junction (STJ) detector with integrated Radio Frequency Single-Electron Transistor (RF-SET) readout amplifier. (See Fig.1). STJs have been used for energy-resolving detection of single photons at visible to x-ray wavelengths[2]. In an STJ detector, a superconducting-insulating-superconducting tunnel junction is biased below its superconducting gap. At temperatures well below the

*Contact information: rob.schoelkopf@yale.edu

Millimeter and Submillimeter Detectors for Astronomy, Thomas G. Phillips, Jonas Zmuidzinas, Editors, Proceedings of SPIE Vol. 4855 (2003) © 2003 SPIE · 0277-786X/03/$15.00

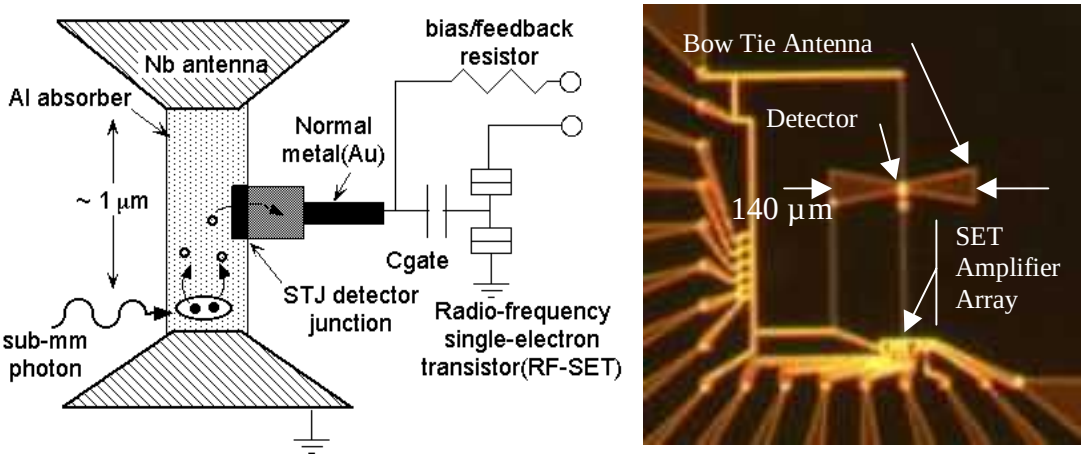

Fig. 1. Single Quasiparticle Photon Counter (SQPC): A niobium bow-tie antenna provides coupling to submillimeter radiation. Absorption of a submillimeter photon breaks Cooper pairs in the aluminum strip joining the halves of the bow-tie, and gives a current pulse through a tunnel junction connected to an RF-SET readout amplifier.

superconducting transition temperature, very little current flows since most electrons are bound in Cooper pairs. The number of thermally-generated unbound quasiparticles, and hence also the dark current and detector noise, decrease exponentially as the operation temperature is lowered. For aluminum junctions, operating temperatures of ≈ 250 mK or less are used.

When a photon is absorbed in one of the superconducting electrodes of the tunnel junction, or in a superconducting absorber film linked to a junction electrode, then much of the photon's energy goes into breaking Cooper pairs, and the quasiparticles released give a current pulse. The integrated charge in the pulse is a measure of the photon energy. At high count rates, overlapping pulses give a photocurrent proportional to the absorbed optical power. The tunneling time which sets the detector speed can be quite fast (≈ 1 μs) since the response is a non-equilibrium effect, and not limited by long thermal phonon relaxation times at low temperatures.

2.1 Use of an STJ detector for low energy photons

Figure 1 shows how an STJ is adapted for detection of millimeter or submillimeter-wave photons in an SQPC. The optimal volume of the STJ detection electrode scales in proportion to the maximum photon energy (see Sec. 4). For submillimeter detection, dimensions of the absorber and junction need to be submicron. Efficient coupling of long-wavelength radiation to the small absorber is provided by an antenna structure. Sensitive and high-bandwidth readout of photocurrents through the small, high-impedance tunnel junction is provided by an integrated RF-SET, as described below.

In our devices, in Fig. 2, we make the STJ using aluminum films for the electrodes and absorber, and we fabricate the antenna from niobium. For photon frequencies between the superconducting gap frequencies of aluminum (100 GHz) and niobium (700 GHz), the aluminum absorber strip appears to have its normal-state resistance, and can present a well-matched impedance for absorbing energy at the center of the superconducting niobium bow-tie antenna.

Figures 1 and 2a show an additional feature: a normal metal (gold) section in the bias lead near the detector junction. This acts a quasiparticle trap which aids rapid diffusion of collected quasiparticles away from the junction after tunneling. This prevents the backtunneling effect[3], which may otherwise slow the detector response time. Figure 2b shows that instead of one junction we actually use two junctions in parallel to form a dc Superconducting Quantum

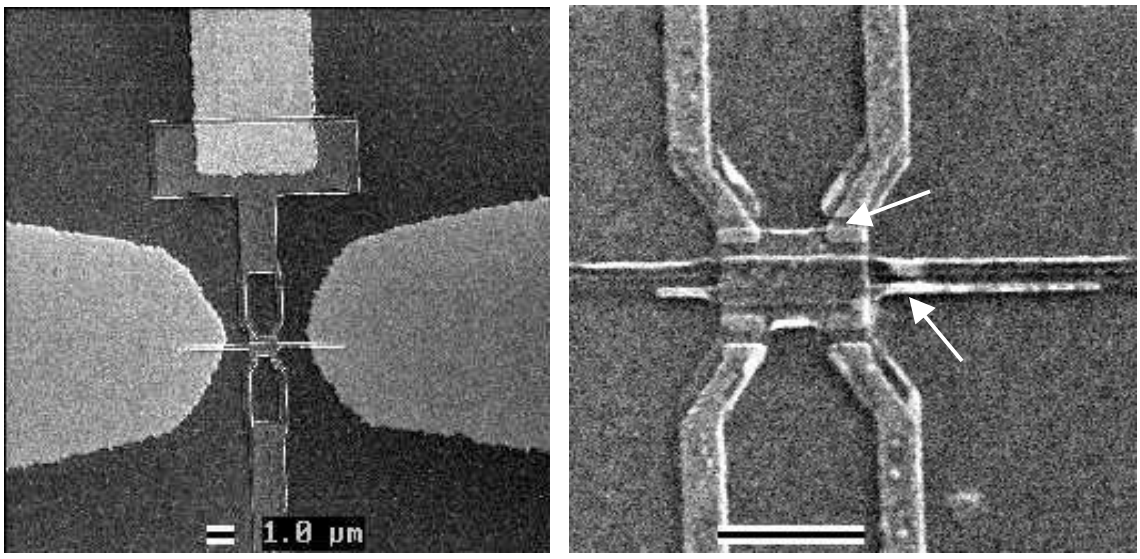

Fig. 2. (a) SQPC detector strip and tunnel junctions are located between two halves of a niobium bow-tie antenna for coupling to submillimeter radiation. A gold quasiparticle trap is included here in the wiring to just one of two dual detector SQUIDs. (b) Close-up view of detector strip and tunnel junctions made by double-angle deposition of aluminum through a resist mask patterned by electron beam lithography. Pairs of junctions form dc SQUIDs, and critical currents can be suppressed with an appropriately tuned external magnetic field.

Interference Device (SQUID). This allows the critical current of the combined junctions to be suppressed nearly to zero, which is necessary for bias stability, and essential for achieving the lowest dark currents (Sec. 3).

2.2 Integrated Readout Amplifier

At detector readout frequencies (<< 100 GHz), the aluminum is superconducting, and the tunnel junction has a subgap differential resistance of 100 MΩ or higher, and a capacitance of a femtofarad or less. A standard readout circuit for a high impedance photoconductor is the transimpedance amplifier (see Fig. 3). An ideal amplifier for implementing this readout circuit for an SQPC is the RF-SET[4]. A Single Electron Transistor (SET) is a very high performance electrometer based on the Coulomb blockade effect[5] with sub-femtofarad input capacitance. An RF-SET[6] integrates the SET with a LC circuit resonant at ≈ 1 GHz to impedance match the typical 50 kΩ SET output impedance to a 50 Ω High Electron Mobility Transistor (HEMT) (located at 4K). Signal bandwidths of 100 MHz can be obtained.

To make an RF-SET transimpedance amplifier, we feed the room temperature output voltage of the RF-SET amplifier system back to the input gate of the SET via a cryogenic, high-value (100 MΩ) resistor integrated at the detector bias point (see schematic in Fig. 1). Although we have not yet done so, we intend to use electron beam lithography to fabricate a feedback resistor on-chip with physical dimensions small enough to not limit the readout bandwidth with stray capacitance.

2.3 Fabrication Process

We use optical lithography and thin-film processing techniques to fabricate substrates for SQPCs and SETs. The substrates include the antenna, inductors and capacitors for the rf circuits, and device contacts.

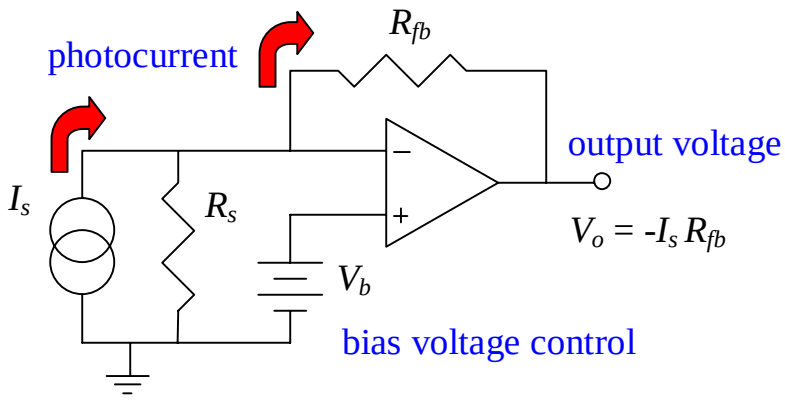

Fig 3. Measuring photocurrent with a transimpedance amplifier: feedback draws photocurrent out through a (cold) feedback resistor, keeping constant bias voltage across the detector.

We use electron-beam lithography to fabricate both SETs and the SQPC detector in one process. Figure 4 shows one of our transistors, and a sketch of the self-aligned process used to form the small tunnel junctions required both for SET and detector. We use a standard SET fabrication process using a resist bilayer[7]. The bottom resist layer is more sensitive to electron-beam exposure than the top, high-resolution layer. Consequently, development of the resists results in undercuts which can be made to merge and form free-standing bridges of the top resist. Evaporating aluminum films onto the substrate at two angles allows junctions to be formed under the resist bridge, as shown in Fig. 4a. A room temperature thermal oxidation step between deposition of the two aluminum layers forms an Al_2O_3 tunnel barrier in the junction area defined by the overlap of the layers.

We have refined this fabrication process with the goal of achieving the reproducibility needed for large-format arrays. By monitoring and controlling the sensitivity of the lower resist layer, we have recently attained large improvements in device yield. We now make chips with 20 or more functional SETs, and small (5 element) arrays of SETs with junction resistances clustered within 10% of a target value. We are continuing to study and make improvements in device yield, uniformity, and long term stability.

3. OPTIMIZATION OF DEVICE PARAMETERS AND EXPERIMENTAL RESULTS

Apart from efficiency of antenna coupling, the fundamental factors determining SQPC sensitivity are: (i) detector responsivity, (ii) shot noise on the dark current, (iii) noise of the RF-SET expressed as an equivalent voltage noise at its input, (iv) Johnson noise in the feedback resistor, and (v) impedance of the detector in parallel with the feedback resistor. We have investigated each of these issues, and predict Noise Equivalent Power (NEP) $\approx 1\times10^{-19}$ W/$\sqrt{\text{Hz}}$ could be obtained with our existing SQPC prototypes based on the demonstrated levels of performance measured for each factor.

3.1 Detector Responsivity

The responsivity of the SQPC is ideally equal to e/Δ, where Δ is the energy gap of the absorber material and e is the electronic charge. For aluminum, $e/\Delta \approx 5000$ A/W. Efficient collection of photon-generated quasiparticles as a tunneling current depends on making the tunneling time short by confining the quasiparticles to a small absorber or trap volume, and on avoiding sources of quasiparticle recombination other than recombination with the thermal equilibrium concentration of quasiparticles. At low operating temperatures, thermal recombination rates are orders of magnitude slower than our 1-10 μs tunneling times. Using the dual detector SQUID structure shown in Fig. 2b, we have used one SQUID in a pair to electronically inject a quasiparticle current into the common absorber strip. We see a strong response in the subgap tunneling current of the second SQUID. While we have yet to complete analysis, we believe the observed response indicates good confinement and collection in our devices.

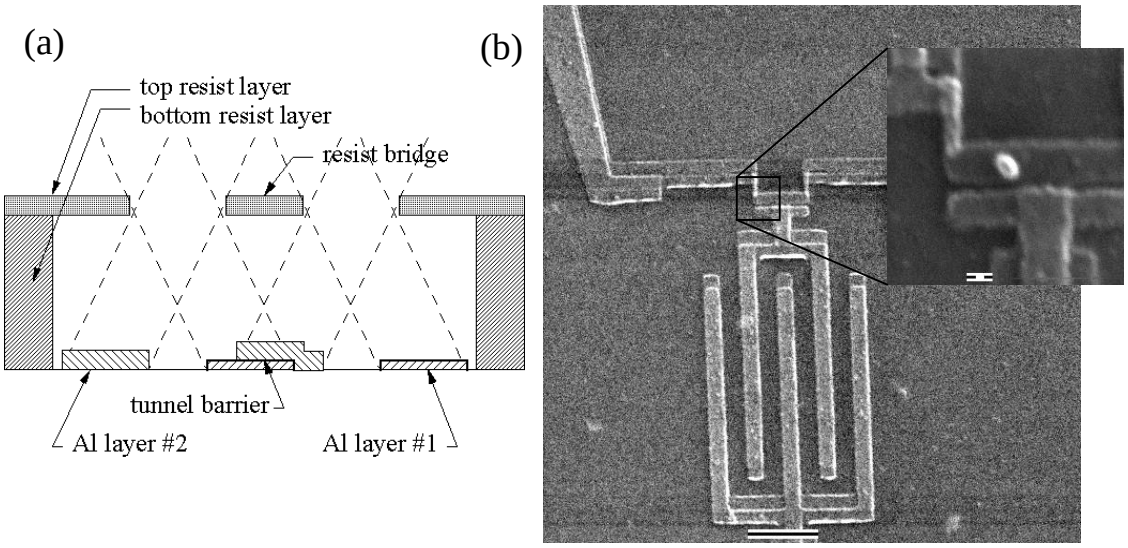

Fig. 4. (a) Double-angle deposition process used to form the self-aligned junctions for the SQPC and SET. (b) An SET with 0.5 fF input gate capacitor. Source and drain leads are connected to island via ultra-small tunnel junctions. Inset shows close up of a 60 nm x 60 nm junction.

3.2 Dark Currents

We have investigated dependence of dark current on device parameters. We found initial prototype detectors with ≈ 1 kΩ junctions deviated from BCS predictions for thermally-generated dark current below ≈ 300 mK. The temperature-independent dark current was proportional to the square of the (magnetic-field dependent) critical current of the SQUID, and was explainable as "rectification" of the Josephson oscillations occurring at a non-zero dc bias voltage[8]. Since the minimum critical current of a dc SQUID is limited to non-zero values by self-inductance, and by asymmetry between junctions, we could not fully suppress the critical current with a magnetic field as is done for UV/optical or x-ray STJ detectors.

Instead, we were motivated to try junctions with smaller areas and higher resistance-area products. For junctions with a Josephson energy $E_J = I_c\Phi_0/2\pi$ smaller than kT, we observed extra suppression of the critical current by thermal fluctuations. The dark current at bias less than Δ/e was then greatly improved. Several different detectors were cooled in a pumped ^{3}He refrigeration system to temperatures as low as 250 mK. Preliminary tests focused on carefully quantifying the dark current and its response to variation in temperature and magnetic field. First, we were able to show that the supercurrent can be suppressed to less than 0.1% on its initial value with a few Gauss of magnetic field on the device. This shows both that the fabrication process can yield sufficiently symmetric SQUID geometries and that we can robustly quench the supercurrent contribution to the dark current.

The next step in our characterization of the junctions was to demonstrate how small the dark current could be and see how this compares with theoretical predictions. BCS theory predicts that the subgap current due to thermally excited quasipartcles should decrease exponentially with temperature. So far, our measurements have shown that the subgap current corresponds to the BCS value and that it continues to scale exponentially at the lowest temperatures at which it has been measured. At 260 mK, we measured a dark current less than 1 pA (Figure 5). This implies that a shot noise limited detector would have an NEP of less than 10^{-19} W/rt.Hz. This sensitivity should continue to improve as the temperature decreases. While it remains to be seen how low this dark current can be made, it is highly encouraging that such a low dark current has been demonstrated and that its value fits so closely with theory.

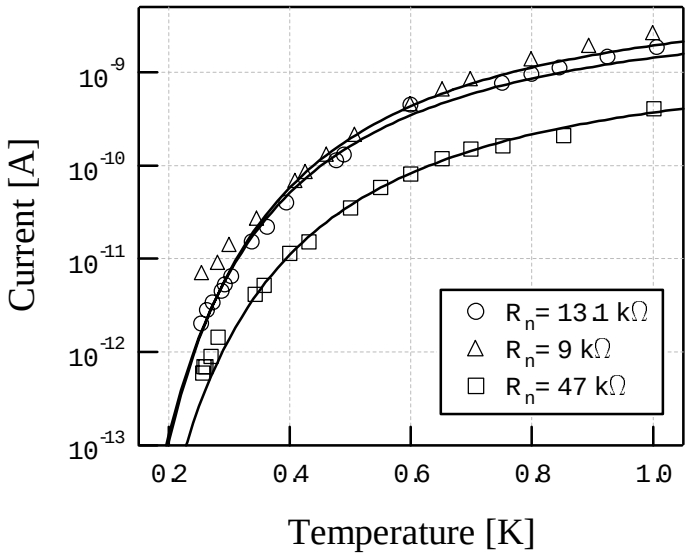

Fig. 5. Data and theory for dark currents of three different detector junctions.

3.3 RF-SET voltage noise

Nearly quantum-limited charge noise $\approx 10^{-6}$ $e/\sqrt{\text{Hz}}$ has been demonstrated for RF-SETs with small input gates[9]. However, just as for dc SQUIDs, it is difficult to maintain quantum-limited sensitivity while providing strong coupling to an input signal. For SQPC readout, the figure of merit is the voltage noise, equal to the charge noise divided by the input gate coupling capacitance. As gate capacitance is increased, the voltage noise at first drops, but then levels off or increases as the charge noise of the RF-SET starts to degrade due to co-tunneling effects[4]. We have obtained record SET voltage noise of 30 nV/√Hz with a 0.5 fF gate, and have been able to maintain a voltage noise close to this value during closed-loop transimpedance amplifier operation[10].

3.4 Predicted Detector Sensitivity

Table I summarizes the noise budget for an SQPC detector using demonstrated parameters. We assume our 0.5 pA device is used with a 100 MΩ integrated feedback resistor at 250 mK, with higher subgap impedance for the biased detector.

Table I. Detector sensitivity for demonstrated parameters.

Noise source	Parameters	Effective current noise
Dark current	0.5 pA at 250 mK	0.4 fA/√Hz
RF-SET noise	30 nV/√Hz	0.3
Johnson noise in Rfb	100 MΩ at 250 mK	0.4
Total current noise		**0.6**
NEP		1.2×10^{-19} **W/√Hz**

4. MODELING OF DETECTOR PERFORMANCE FOR VARIOUS ABSORBED POWER LEVELS

The maximum power level the SQPC can tolerate, and the expected background count rates in a space environment, will determine the maximum fractional bandwidth allowed for the incident radiation. As the absorbed power is

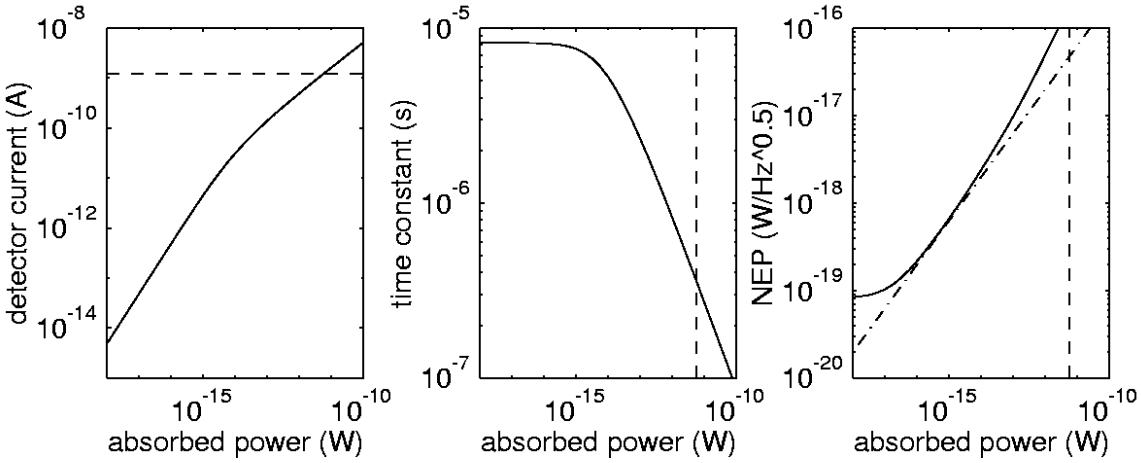

Fig. 6. Simulated saturation effects for 300 GHz photons absorbed in an SQPC with 40 kΩ normal resistance, 0.023 $(\mu m)^3$ absorber volume. Plots show power dependence of photocurrent, time constant, and NEP. Dash-dot line shows limiting NEP from just photon shot noise. Dashed lines estimate current or power levels at which device will be driven normal.

increased, the peak or steady-state concentration of quasiparticles in an SQPC absorber strip will grow, and the rate of self-recombination of particles will increase. When the self-recombination rate per quasiparticle equals or exceeds the tunneling rate, then the efficiency of charge collection drops. We have performed Monte Carlo simulations of the effects on signal and noise in this case, and have found that the saturation of the detector is really quite gradual and weak. Preliminary results calculated for a device like our prototype with 0.5 pA dark current. The self-recombination and tunnel times become equal at an absorbed power of 3 fW. Above that power, the photocurrent grows as square-root of power, and the time constant of the response drops with the self-recombination time. The total NEP degrades very slowly, and remains close to the photon shot-noise limit until the power reaches 0.1 pW. With the expected background for space observations[11], this SQPC model allows background limited sensitivity for incident bandwidths of 0.1% to 100%. Only at powers above a pW will the device saturate "hard," when quasiparticle concentrations grow large enough to supress the superconducting gap and drive the aluminum normal. We consider weak saturation one advantage of the SQPC.

5. DESIGN OF ANTENNA COUPLING AND CALIBRATION

We have an experiment currently underway to attempt to measure for the first time the photoresponse of an SQPC to radiation. For this purpose, we have made a calibrated 200 GHz source with calculable coupling to the SQPC antenna.

5.1 STJ/Antenna Coupling

At this stage of sensor development, we employ a bow-tie antenna on a dielectric substrate to optically couple the device. This simple scheme has minimal impact on processing and will allow basic characterization of the device properties. In order to integrate the detector to the antenna, the impedance, field configuration, and interaction of the bias network topology with the radiating structure need to be considered.

We estimate the bow-tie antenna's input impedance by treating the structure as a radial transmission line in the quasi-static limit[12]. For the geometry used for the prototype devices, we estimate an input impedance of ~130 Ω. The rf

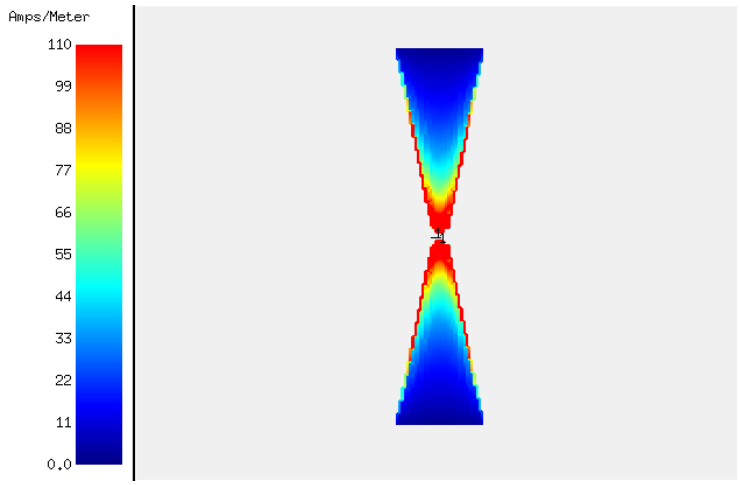

Fig. 7. Simulation of bow-tie antenna high-frequency current distribution.

impedance presented by a typical SQPC-SET sensor is 20~50 Ω. This impedance mismatch will be addressed in subsequent sensor iterations.

For an antenna on a substrate, the power radiated into the dielectric is greater than the power radiated into the vacuum by a factor of $e_r^{-1.5}$. For the silicon substrate in use, we note that ~97.5% of the power resides in the dielectric portion of the half-space. A quarter-wave-matching layer is employed between the dielectric and freespace to improve the coupling efficiency for the component of the radiation propagating away from the antenna into the dielectric. A substrate lens can also be employed to limit conversion of trapped rays into surface waves on an electrically thick substrate.

The beam efficiency, the ratio of the main beam-to-total beam solid angle, for a bow tie is relatively low. For this reason, we plan to transition to antenna structures with improved sidelobe control. This will enhance compatibility of the device development effort with needs of precision radiometric applications. Given the sensor's planar topology, processing requirements and RF impedance levels; dual slot and taper slotline configurations are presently under consideration to meet these demands.

5.2 200 GHz Calibration Source Development

A quasi-optical calibration scheme was chosen to allow maximum flexibility during sensor characterization. For the initial measurements, a quasi-optically coupled "reverse bolometer" will be used as a thermal source in the sensor's field of view to produce a calculable radiometric flux. The absorber physical temperature and emissivity as a function of frequency effectively control the source bandwidth.

The calibrator was fabricated as follows: The absorber was formed by evaporation of Pd/Au to realize ~400 Ω/□ on an electrically thin silicon substrate at the anticipated operational temperature. This layer is held in a silicon frame at a spacing of ~410 microns, roughly a quarter wavelength, from a smooth oxygen free copper backshort. The emitter is supported on micro-machined conductive legs, which provide electrical connections for the thermometry and thermal isolation. Provisions are provided in the design to reconfigure the calibrator for use as a mount in WR05 waveguide for verification of the coupling efficiency via standard waveguide metrology techniques.

6. MULTIPLEXING FOR ARRAYS

An advantage we see for the SQPC detector system is the multiplexing capability of RF-SETs. Multiplexing schemes will be crucial to the development of large-format arrays of SQPCs, or other low-temperature detectors.

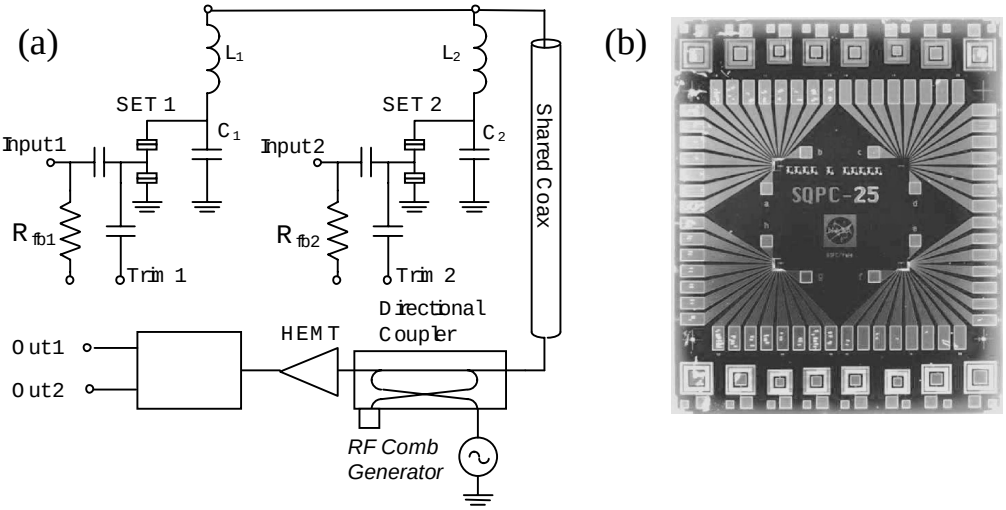

Fig. 8. (a) WDM multiplexing scheme. All inductors are connected to one coax running from subkelvin chip to components at 4K. Multiple carrier frequencies pass through directional coupler to excite tank circuits. Reflected power is directed to HEMT amplifier. Outputs are demultiplexed and demodulated at room temperature, and fedback to resistors for transimpedance operation. Detector bias can be changed using trim gates. (b) 8 mm x 10 mm chip with 16 lithographically defined tank circuit inductors.

RF-SETs have a natural wavelength division multiplexing capability, as shown in Fig. 8a. Each RF-SET is connected to one coaxial line by an rf tank circuit with a unique resonance frequency. A directional coupler allows rf carriers to be applied at each resonance frequency and reflected powers to be monitored by a single HEMT following amplifier at 4 K. RF-SETs can be individually or simultaneously powered and read out. We have made a two-channel rf multiplexing demonstration using discrete inductors for the rf tank circuits[4]. The two input signals were successfully reconstructed with little cross-talk. Lithographic versions of the rf circuits (Fig. 6b) had measured parameters in agreement with electromagnetic modeling, with reduced cross capacitance and inductance. We have designed a 50-channel system with components based on measured parameters of our lithographic circuits[13].

The wavelength division multiplexing scheme still requires two wires for each pixel which is being read out simultaneously: one wire for connection to the transimpedance feedback resistor, and one for a weakly coupled SET trim gate. Combining wavelength division multiplexing with some form of time-division, or other, multiplexing will be required in to implement large arrays; however, the 50-fold reduction in output connections seems quite valuable.

7. CONCLUSION

We have refined a fabrication process for SQPC detectors and RF-SET amplifiers with the goal of achieving the reproducibility needed for large-format arrays, and have recently attained large increases in device yield. With proper device design, we have attained subpicoamp dark currents, and record RF-SET voltage noise levels, which allow sensitivities of 1×10^{-19} W/$\sqrt{\text{Hz}}$ at temperatures as high as 250 mK. There is potential for even better sensitivity at lower temperatures, and the expected detector saturation behavior and multiplexing capability of RF-SETs enhance the potential for application of the SQPC in space-based submillimeter-wave interferometers.

8. ACKNOWLEDGMENTS

This work has been funded by GSFC Director's Discretionary Funds, NASA Explorer and CETD Programs, NASA Codes S & R, NASA NSG-8589.

9. REFERENCES

1. R. J. Schoelkopf, S. H. Moseley, C. M. Stahle, et al., IEEE Trans. Appl. Supercond. **9** 2935, 1999.
2. A. Peacock, P. Verhoeve, N. Rando, A. van Dordrecht, B. G. Taylor, et al., Nature **381** 135, 1996.
3. C. M. Wilson, L. Frunzio, K. Segall, L. Li, D. E. Prober, et al., Trans. Appl. Supercond. **11** 645, 2001.
4. T. R. Stevenson, A. Aassime, P. Delsing, et al., IEEE Trans. Appl. Supercond. **11** 692, 2001.
5. T. A. Fulton, G. J. Dolan, Phys. Rev. Lett. **59** 109, 1987.
6. R. J. Schoelkopf, P. Walgren, A. A. Kozhevnikov, P. Delsing, D. E. Prober, Science **280** 1238, 1998.
7. G. J. Dolan, Appl. Phys. Lett. **31** 337, 1977.
8. T. Holst, D. Esteve, C. Urbina, M. H. Devoret, Physica B **20**3, 397, 1994.
9. A. Aassime, D. Gunnarsson, K. Bladh, P. Delsing, R. Schoelkopf, Appl. Phys. Lett. **79** 4031, 2001.
10. K. Segall, K. W. Lehnert, T. R. Stevenson, R. J. Schoelkopf, 2002, submitted to Appl. Phys. Lett.
11. J. C. Mather, S. H. Moseley, D. Leisawitz, et al., astro-ph/9812454, 1998.
12. D. B. Rutledge, M. S. Muha, IEEE Trans. Antennas Propag., **AP-30** 535, 1982.
13. T. R. Stevenson, F. Pellerano, C. Stahle, K. Aidala, R. Schoelkopf, Appl. Phys. Lett. **80,** 2002.